Identification of NOX2 regions for normal biosynthesis of cytochrome b558 in phagocytes highlighting essential residues for p22phox binding

Sylvain Beaumel, Didier Grunwald, Franck Fieschi, Marie José Stasia

Identification of NOX2 regions for normal biosynthesis of cytochrome b_{558} in phagocytes - Highlighting essential residues for p22^{phox} binding

Sylvain Beaumel[*†], Didier Grunwald[‡], Franck Fieschi[§ǁ¶] and Marie José Stasia[*†1]

[*]Chronic Granulomatous Disease Diagnosis and Research Centre, Therex-TIMC/Imag, UMR CNRS 5525, Univ. Grenoble Alpes, Grenoble, F-38041, France, [†]Pôle Biologie, CHU de Grenoble, Grenoble, F-38043, France, [‡]iRTSV/CEA, 17 rue des Martyrs, 38054 Grenoble Cedex 9, France, [§]Univ. Grenoble Alpes, Institut de Biologie Structurale (IBS), F-38044 Grenoble, France, [ǁ]CNRS, IBS, F-38044 Grenoble, France, [¶]CEA, DSV, IBS, F-38044 Grenoble, France

ABSTRACT

Cytochrome b_{558}, the redox core of the NADPH-oxidase complex in phagocytes, is composed of NOX2 and p22^{phox} whose synthesis are intimately connected but not fully understood. We reproduced ten rare Xminus chronic granulomatous disease mutations of highly conserved residues in NOX1–4, in the X^{0}CGD PLB-985 cells in order to analyse their impacts on the synthesis process of cytochrome b_{558}. According to the impact of these mutations on the level of NOX2 expression and activity, mutants were categorized in group A (W18C, E309K, K315del, I325F) characterized by a linear relationship between NOX2 expression and the NADPH oxidase activity and group B (H338Y, P339H, G389A and F656-F570del) showing an absence of NADPH oxidase activity associated with variable levels of NOX2 expression. These last residues belong to the FAD-binding pocket of NOX2, suggesting this functional domain plays a role also in the structural integrity of NOX2. Finally, we observed an abnormal accumulation of p65-kDa, the NOX2 precursor and a p65-kDa/p22^{phox} dissociation in the W18C, E309K, I325F and G389A mutants, pointing out a possible role of the first transmembrane domain (W18) and the region between the membrane and the dehydrogenase domain of NOX2 (E309, I325, G389), in the binding with p22^{phox}.

Keywords: cytochrome b_{558}; NOX2; precursor p65-kDa; biosynthesis; X^{minus} CGD; p22^{phox}

Summary statement: X$^-$CGD mutant analysis provides the first indications on NOX2 regions essential for the normal cytochrome b_{558} synthesis in phagocytes; the FAD-binding pocket, the first transmembrane passage and a cytosolic region located between the membrane and the dehydrogenase domain of NOX2.

Abbreviations used : NOX, NADPH oxidase; ROS, reactive oxygen species; CGD, chronic granulomatous disease; PMA, Phorbol 12-myristate 13-acetate; fMLP, formyl-methionylleucyl-phenylalanine; Cytb_{558}, cytochrome b_{558}; DMF, dimethylformamide; DFP, diisopropylfluorophosphate; DPI, diphenylene iodonium; INT, iodonitrotetrazolium, SOD, superoxide dismutase; O_2^-, superoxide; G6PD, Glucose 6 Phosphate Dehydrogenase.

[1] Correspondence may be addressed to: Marie José Stasia, Pharm D, PhD, CDiReC, Institut de Biologie et Pathologie, CHU de Grenoble, BP 217, 38043 Grenoble Cedex 9 France.
Fax: 33476765608; E-mail: mjstasia@chu-grenoble.fr

INTRODUCTION

Phagocytes, essentially monocytes, macrophages and neutrophils, exert the crucial physiological function of ingesting foreign bodies, including microbes, and cellular debris. Although phagocytes have other microbicidal mechanisms including the secretion of antimicrobial peptides (e.g. defensins) and broadly acting proteases, phagocytosis, with the generation of reactive oxygen species (ROS) by the NADPH oxidase complex, is still regarded as the critical mechanism for killing most invading pathogens. Indeed, the phagocyte NADPH oxidase plays a crucial role in the host's defense against invading microorganisms by catalyzing the formation of superoxide (O_2^-), which is the precursor of a variety of microbicidal oxidants such as hydrogen peroxide (H_2O_2) (1). The importance of this enzyme in innate immunity and inflammation is illustrated by chronic granulomatous disease

(CGD), a rare inherited syndrome (frequency, about 1/200 000) characterized by the absence of NADPH oxidase activity, severe and recurrent infections in childhood and chronic inflammatory granuloma (2). This enzyme is dormant in resting cells but becomes activated during phagocytosis to produce superoxide. Indeed its activity is subtly controlled by a dynamic assembly process involving several cytosolic proteins ($p40^{phox}$, $p47^{phox}$, $p67^{phox}$, Rac1/2) and a membrane partner which is the catalytic component of this protein complex, the flavocytochrome b_{558} (cytb_{558}). The cytb_{558} is composed of a small subunit, $p22^{phox}$, and a larger one, the glycosylated flavocytochrome $gp91^{phox}$ or NOX2, closely associated in the plasma membrane or in the membranes of specific granules (3). NOX2 is the redox element of the NADPH oxidase complex containing hemes (4) and flavin centers that mediate electron transfer from NADPH to molecular oxygen, ultimately resulting in the production of oxidizing species involved in the destruction of phagocytosed microorganisms. In the last decade, homologues of NOX2 have been identified, including four additional proteins (NOX1, NOX3, NOX4 and NOX5) and two dual oxidases (DUOX1 and DUOX2) (5). These homologues all share a common structure with NOX2. Although NOX2 has, as yet, never been crystallized, some information about its function is available (6). The N-terminus of NOX2 is intracellular (7) and is followed by six membrane-spanning domains that are potential α-helices, which contain two heme groups ligated by four histidine residues in the III^{rd} and V^{th} transmembrane passages (8), three glycosylated asparagines in two external loops C and E (9), and the B and D intracellular loops.

Nevertheless, the regions of NOX2 that are important for its synthesis and stability have not been determined. Indeed, the synthesis of cytb_{558} is a complex process because it involves not only the presence of both subunits, NOX2 and $p22^{phox}$, but also several maturation steps, including heme incorporation, heterodimer formation and the glycosylation of NOX2 (10,11,12. Moreover, in primary cells, the heterodimerization, translocation and enzymatic function of NOX2 but also of NOX1,3 and 4, require the presence of p22phox, NOX5 being an exception{Bedard, 2007 #14). Previous studies showed that NOX2 is cotranslationally glycosylated and first detected as a high mannose 65-kDa (p65) monomer in the endoplasmic reticulum (ER) even in the absence of $p22^{phox}$. Full maturation of NOX2 requires sequential incorporation of heme into p65, heterodimerization with $p22^{phox}$ occurring in the late ER step and final N-glycosylation in the Golgi, which drives the transport of the complex to the plasma membrane and into specific granules in neutrophils (13). However, heme insertion is decisive for the stable formation of the heterodimer, whereas glycosylation is not. The association of NOXs with $p22^{phox}$ seems to be a prerequisite for the localization of the heterodimer to specific membrane compartments such as the perinuclear vesicles for NOX4 and plasma membranes in the case of NOX1, 2 and 3 [16]. The importance of some sequences of $p22^{phox}$ for its interaction with NOXs has been highly debated (14-17). However, the binding regions of NOX2 that interact with $p22^{phox}$ are not yet known.

One way to decipher the molecular mechanism of cytb_{558} synthesis, and to identify decisive regions of NOX2 involved in its maturation, is to study this process in special X-linked chronic granulomatous (CGD) disease variants called Xminus (X^-). X^--CGD mutants are characterized by a partial defect of cytb_{558} synthesis associated with no or diminished oxidase activity. These mutants have helped to highlight regions of NOX2 essential for its stable synthesis. The genetic defects in *CYBB* found in these variants are often missense mutations or small deletions located in the coding region (18). The clinical severity of this disease in patients is variable and is probably related to the residual oxidase activity found in the patients' X^--CGD neutrophils. Indeed, X^--CGD mutations could have a different impact and act at different steps of the cytb_{558} synthesis process, and probably affect this synthesis differently. When we started this project, a few X^--CGD mutations were listed in the literature (19). The level of NOX2 or cytb_{558} expression and the NADPH oxidase activity were reported in half of these mutations (H101Y, A156T, S193F, C244S, C244Y, E309K, K315del, H338Y, P339H, G389A, V534_G538del and F565_F570del) in neutrophils or in Epstein-Barr immortalized B lymphocytes (EBV-LB) from CGD patients (20-29). Others were documented only in reviews which list cases of X-linked CGD (W18C, A53D, C59F, K161R, I187_I189del, I325F and V534_G538del) (19,30-35). The impact of these mutations at the molecular level cannot be studied because of the limitation in the amount of biological material. The molecular mechanism of the defect of cytb_{558} synthesis has been highlighted in only two of them (23) (36) (37). The H338Y mutation leads to a defect in FAD incorporation in neutrophils of the X^--CGD patient, highlighting the importance of the ^{338}HPFT^{341} motif of NOX2 in the binding of the isoalloxazine ring of FAD and its

importance in NOX2 stability. In addition, this mutation leads to ER retention related to a partial defect of NOX2 maturation (38). The defect in cytb_{558} synthesis caused by the H101Y mutation was also explained by the absence of heme incorporation in NOX2 because this histidine is one of the four that coordinate hemes in NOX2 (24). Thus this mutation probably prevents NOX2 and p22*phox* interaction, stopping cyt*b* synthesis. However, this was not demonstrated in the X$^-$-CGD patient neutrophils initially published.

Despite recent progress, additional work is needed to improve our understanding of the overall domain structure of NOX2 involved in cytb_{558} biosynthesis, most particularly the regions involved in p22^{phox} binding. Therefore, we decided to study the functional and molecular impact of certain X$^-$-CGD mutations that have never been or only partially characterized using transgenic PLB-985 cells mimicking X$^-$-CGD neutrophils. A better knowledge of the cytb_{558} synthesis process and its relationship with the level of NADPH oxidase activity will help us to better understand the variability of the clinical severity of X$^-$CGD variants.

MATERIALS AND METHODS

Materials

The materials used were: Phorbol 12-myristate 13-acetate (PMA), dimethylformamide (DMF), diisopropyl-fluorophosphate (DFP), actinomycin D, pepstatin, leupeptin, phenylmethylsulfonyl fluoride (PMSF), and Hoechst 33258 (Sigma Chemical Co); Foetal bovine serum, RPMI 1640, Alexa Fluor 488 goat-F(ab')$_2$ fragment anti-mouse IgG1 (H+L) (ref A21121) and Cyanin5 goat-F(ab')$_2$ fragment anti-rabbit IgG (H+L) (ref A10523) (Life Technologies); 7D5 (ref D162-3, Clinisciences); Anti-Lamin B1 (ref Ab 16048), Anti-GM130 (ref Ab 52649), Anti-Calnexin antibodies (ref Ab 22595, Abcam); anti-NOX2 54.1 (ref sc-130543), goat anti-mouse IgG-HRP, monoclonal antibody CS9 (anti p22^{phox}) (sc-130551, Santa Cruz Biotechnology); monoclonal antibodies 48 (anti-NOX2, MW1842) and 449 (anti-p22^{phox}, MW1843) (Sanquin Research at CLB Amsterdam); Geneticin (GE Healthcare); Endofree plasmid Maxi Kit, QIAprep Spin Miniprep Kit (Qiagen); The Sephaglas kit and molecular weight markers (Page Ruler®) (Amersham) and (Fermentas); Nitrocellulose sheets for Western blotting (Bio-Rad).

Site-directed mutagenesis and expression of recombinant NOX2 in the X$^-$CGD PLB-985 cell line

Site-directed mutagenesis was performed with the Quick Change^{TM} Mutagenesis Kit (Stratagene) according to the manufacturer's instructions, using two sets of complementary oligonucleotides harbouring the desired mutation. DNA sequences were verified by DNA sequencing on both strands using the Big Dye Kit (Eurofins). The wild type or mutated gp91^{phox} cDNA were then sub-cloned into the mammalian expression vector pEF-PGKneo (39). The X^0-CGD PLB-985 cell line (lacking NOX2 expression and NADPH oxidase activity) (40) was transfected with the pEF-PGKneo constructs by nucleofection (Amaxa) and clones were selected by limiting dilution.

Cell culture and granulocyte differentiation

Transfected PLB-985 cell lines were grown in RPMI-1640 supplemented with 10% (v/v) fetal bovine serum, 100 units/mL penicillin, 100 µg/mL streptomycin, and 2 mM L-Glutamine at 37°C in a humidified 5% CO_2 atmosphere. Geneticin (0.5 mg/mL) was added to maintain the selection pressure of the plasmid in the transfected cells. For granulocytic differentiation, PLB-985 cells (2×10^5 cells/mL) were exposed to 0.5% (v/v) dimethylformamide for 6 days (41). Geneticin (0.5 mg/mL) was added to maintain the selection pressure in the transfected cells.

Analysis of recombinant NOX2 expression in PLB-985 cell lines

NOX2 expression was analysed using flow cytometry and immunoblot in transfected PLB-985 cell lines as described previously (42). 5.0×10^5 PLB-985 cells labelled with 5 µg/ml of monoclonal 7D5 or irrelevant IgG1 and then incubated with phycoerythrin-labelled goat-F(ab′)$_2$ fragment anti-mouse IgG (Beckman Coulter) were analysed by Flow cytometry with a FACSCanto II (BD Biosciences) [42]. We detected 15–20 different clones for each mutant, and to minimize clone-to-clone variation in NOX2 expression, two to three independent clones of each X$^-$-CGD mutant were used for subsequent analysis (data not shown). The purity of the clonal population was higher than 97%. Expression of

NOX2, its precursor p65-kDa, $p22^{phox}$ and $p47^{phox}$ were examined by Western blot analysis (43,44) using monoclonal antibodies 48, 449 and anti-$p47^{phox}$ (ref 610354 BD Biosciences) respectively (45,46). Polyclonal goat anti-mouse IgG-HRP was used as a second antibody and the immune complexes was detected by chemiluminescence using an ECL kit Femtomax (Rockland Immunochemicals).

Measurement of ROS production by chemiluminescence

ROS production by intact differentiated PLB-985 cells (5×10^5 cells) in PBS containing 0.9 mM $CaCl_2$, 0.5 mM $MgCl_2$, 20 mM glucose, 20 µM luminol, and 10 U/mL HRPO was measured after PMA stimulation (77 ng/mL). Relative light units (RLUs) were recorded at 37°C over a time course of 60 min in a Mithras LB 940 (Berthold Technologies) (42).

Analysis of NOX2/p65-kDa location in subcellular compartments of X^-CGD PLB-985 cells by confocal microscopy

The differentiated PLB-985 cells (5×10^5) were deposited on coverslips at 37°C for 15 min then fixed in 4% formaldehyde for 10 min and permeabilized with 0.25% Triton X 100. After extensive washing, cells were incubated for 1 h at 37°C with diluted 54.1 anti-NOX2 monoclonal antibody, and the rabbit polyclonal antibodies directed against calnexin in the endoplasmic reticulum, the rabbit monoclonal directed against GM-130 in the Golgi or the rabbit polyclonal directed against lamin B1 in the nuclear membrane. All primary antibodies were diluted at 1/100 and secondary antibodies at 1/200. After washing, cells were incubated in 5% BSA/PBS buffer containing 2 µg/mL Alexa Fluor 488 $F(ab')_2$ fragments of goat anti-mouse IgG (H+L) and cyanin5 $F(ab')_2$ fragments of goat anti-rabbit IgG (H+L) used as second antibodies. Cellular nuclei were visualized using Hoechst 33258 staining. Cells were examined with a confocal laser scanning microscope and analysed using Leica confocal software (42).

Preparation of the Triton X100 soluble extract from X^-CGD PLB-985 cell lines

Differentiated PLB-985 cells were harvested by centrifugation (1000 *g* for 10 min at room temperature) and treated with 3 mM diisopropyl-fluorophosphate (DFP) for 15 min on ice. After centrifugation, the cells were resuspended at 1×10^8 cells/mL in the lysis buffer A (1% Triton X100 (v/v), HEPES 10 mM, $MgCl_2$ 3.5 mM, 1 mM phenylmethylsulfonyl fluoride (PMSF), 4 µM leupeptin and 4 µM pepstatin) for 30 min on ice (47). After centrifugation, the soluble extract was recovered in the supernatant and the protein content was estimated using the BCA Protein Assay (Interchim).

Co-immunoprecipitation of p65-kDa and $p22^{phox}$ from X^-CGD PLB-985 membrane fractions

Soluble extract (SE) (100 µg) was incubated with mAbs CS9 directed against $p22^{phox}$ (2 µg) in 500 µL of buffer A for 30 min on ice. We added 100 µL of µMACS protein G MicroBeads (Miltenyi Biotec, Paris, France) and incubated the solution for 30 min on ice. The sample was loaded onto a MACS Column placed in the magnetic field of the µMACS Separator. The magnetically labelled antibody–protein complex and associated molecules were retained on the column and the flow-through (−) was recovered. After washing, 50 µL pre-heated (95°C) gel loading buffer (50 mM Tris HCl (pH 6.8), 50 mM DTT, 1% SDS, 0.005% bromophenol blue, 10% glycerol) were loaded onto the column matrix for elution of the (co-)immunoprecipitated proteins as the positive fraction (+), which was recovered. The protein content of flow-through (-), positive and initial soluble extract fractions (100 µg of proteins in each sample), was assessed by immunoblot analysis as described above. IgG1 antibodies were used as irrelevant antibodies.

Protein determination

Protein content was estimated by the Pierce method using a Bio-Rad protein-assay kit II and bovine serum albumin as standard (48).

cDNA generation by reverse transcription amplified by PCR (RT-PCR)

Total RNA was isolated from cells using a modified single-step method (49),(50). cDNA was synthesized from 5 µg of total RNA by the reverse transcriptase reaction according to the manufacturer's instructions (QBiogen, Montréal, Canada). NOX2 or p22*phox* cDNA were immediately amplified by the polymerase chain reaction (PCR) using specific primers (27). RT-PCR

was performed with geneticin primers as a control for RNA quality and equal loading. Aliquots of 5 µL PCR products in bromophenol blue solution were run together with a DNA ladder (markers XIV, Roche Diagnostics, Indianapolis, IN, USA) on 1% (wt/vol) agarose. The bands were photographed under UV light (Gel Doc XR$^+$, Bio-Rad).

Quantitative PCR

Real-time ready assays were conducted with the LightCycler® 2.0 Instrument according to the manufacturer's instructions (Roche). Total RNA was extracted from differentiated X--CGD PLB-985 cells treated or not with actinomycin D 5µg/mL for 4 h as previously described (51). qPCR reactions were performed using Faststart Taqman probe master 1x (Roche, ref 4707494001) in 20 µL reaction volume with 10 ng cDNA/RNA, specific primers forward and reverse (500 nM each) of NOX2 and the reference gene (*G6PD*). Specific probes (250 nM each) of NOX2 and G6PD were labeled with FAM and Yellow 555, respectively. Reaction conditions were: +95°C for 10 min, 40 cycles of +95°C for 10 s, +59°C for 30 s (with single acquisition) followed by +40°C for 30 s final cooling. Color compensation was applied between specific emission of FAM (530 nm) and Yellow 555 (560 nm). Relative gene expression was calculated according to the ΔDCt method12 using the LightCycler® 2.0 Software with normalization to the G6PD RNA level as the endogenous reference. Normalized values represent average ± SD of at least four independent experiments.

RESULTS

Position and conservation of X$^-$-CGD mutated amino acids in the NOXs

Approximately 30 mutations leading to X$^-$-CGD cases, characterized by a lower level of cytb_{558}, have been described in the literature to date (see Roos et al. [35] for a review]. As can be seen in Figure 1A according to their location in the NOX2 protein, four distinct regions are hot-spots; the second intracellular loop D, a cytosolic region close to the last transmembrane passage VI, the FAD-binding site and the extreme N terminal region of NOX2. We concluded that these regions were probably highly involved in the stability or the synthesis/maturation process of cytb_{558}. However until now, the majority of these mutations have been classified as X$^-$-CGD mutations on the grounds of the NADPH oxidase activity and cytb_{558} expression in the patients' neutrophils, or their inclusion as X$^-$-CGD in reviews without any other information. Therefore, we reproduced some X$^-$-CGD mutations within these regions (I187_I189del, E309K, K315del, I325F, H338Y, P339H, F565_F570del) and in isolated regions (W18C and G389A) in the X^{0}CGD PLB-985 cell line, in order to decipher the role played by these residues in the synthesis process of cytb_{558}. The H101Y mutation, which is one of the binding His of the hemes, was also reproduced because it serves as a control of the heme incorporation defect leading to the absence of NADPH oxidase activity and probably binding of its precursor p65kDa with p22^{phox}, as was demonstrated previously by treatment with a heme synthesis inhibitor [28]. The orientations of the mutations were also chosen because of the high conservation of these mutated residues in NOX1 to NOX4 (Figure 1B), suggesting a common and important role, possibly in the interaction with p22^{phox}.

Characterization of the NOX2 expression in the X$^-$-CGD PLB-985 mutant cells

The first challenge was to exactly reproduce the phenotype of X$^-$-CGD human neutrophils in the transfected X^{0}CGD PLB-985 cell line. To be sure that the defect of NOX2 expression in X$^-$-CGD mutant cells was not due to a defective transfection, mutated NOX2 mRNA was quantified by RT-PCR by comparing it with the amplification of the geneticin resistance gene located in the plasmid used to clone the mutated NOX2 cDNAs (Figure 2A). A nearly equivalent level of NOX2 mRNA was transcribed in mutant PLB-985 cells. This confirmed the correct transfection and transcription of the mutated cDNAs NOX2 and p22^{phox} mRNA. To confirm these previous data and to test NOX2 mRNA stability, we used real-time PCR to measure the amount of NOX2 mRNA of the mutant PLB-985 cells before and after treatment with actinomycin D 5 µg/mL for 4 h (Figure 2B). We also observed that all the mutants except H101Y, I325F and P339H have 50% or less steady state mRNA levels compared with WT-NOX2. While this likely cannot explain the greater decreases in cell surface protein, it could contribute to it. However we found that the values for the transfected PLB-985 cells (WT-NOX2 or

mutated NOX2 cDNA) were always higher than the values obtained for the human neutrophils (PMN) and the WT PLB-985 cells. In addition, no difference between group A and group B mutants (as classified in Table 1) was observed. The actinomycin treatment slightly affected the level of mRNAs, suggesting good stability of the mutated NOX2 mRNA. These results suggest that X^-CGD mutations do not affect the transcription step drastically but they could probably influence later stages during protein synthesis.

NOX2 expression at the plasma membrane of undifferentiated and differentiated PLB-985 cells was checked by flow cytometry using the 7D5 monoclonal antibody. A striking point was that the membrane NOX2 expression diminished in differentiated mutant PLB-cells compared to undifferentiated mutant PLB-985 cells (Figure 3A). The entire human CGD X^--mutations were reproduced in the PLB-985 cell model except the I187_I189del where no NOX2 expression was observed as an X^0-CGD phenotype. In order to analyse the total NOX2 expression of the mutant cells (at the plasma membrane plus in intracellular compartments), Western blot analysis was performed from each mutant cell line (Figure 3B). This method makes it possible to analyse not only the total NOX2 expressed in the cells, but also its precursor of p65-kDa and $p22^{phox}$ to be visualized. However the levels of proteins' expression seen in the western blot of undifferentiated and differentiated cells, cannot be compared because both results from unequal times of exposure. $P47^{phox}$ was revealed in order to normalize the quantification of protein expression. The level of NOX2 expression was variable in all the mutants and corresponds to what we found with flow cytometry except for the H338Y and P339H mutants (Table 1, Figure 3B). Indeed the total amount of NOX2 assessed from Western blot (46.4% and 38% of the control cells, respectively) was considerably higher than those measured by flow cytometry (10% and 5% of the control cells, respectively). This suggests an intracellular location of NOX2. In addition, the level of $p22^{phox}$ expression seems to mimic the level of NOX2 when it is expressed. In some mutants (W18C, E309K, I325F, E389) there is an accumulation of the precursor p65-kDa (Table 1, Figure 3B) and the ratio p65/NOX2 is higher than in WT NOX2 cells (5, 6, 18 and 27, respectively) (Table 1).

NADPH oxidase activity in X^-CGD PLB-985 mutant cells

The NADPH oxidase activity was measured in all X^--CGD mutant PLB-985 cells using chemiluminescence in the presence of luminol and HRPO as described in the Material and Methods section. As seen in Table 1, in group A mutants there was a faint residual NADPH oxidase activity (W18C, E309K, K315del, I325F), whereas in group B mutants the NADPH oxidase activity was totally abolished (H338Y, P339H, G389A and F565_F570del). In addition, in group A mutants, the level of NOX2 expressed at the plasma membrane measured by flow cytometry was directly proportional to the level of NADPH oxidase activity (Table 1). This suggests that these X^--CGD mutations lead to a defect in the efficiency of the cytb_{558} synthesis process only and do not affect the intrinsic NADPH oxidase activity. However, in the group B mutants, the NADPH oxidase activity was null, whereas NOX2 was expressed at the plasma membrane at levels between 2 and 12% of that seen in controls. In this case, the X^--CGD mutations affecting not only cytb_{558} synthesis, but also the NADPH oxidase activity point to functional regions of NOX2 that are essential for the stable conformation of the protein.

Cellular location of NOX2 and p65-kDa in X^-CGD PLB-985 mutant cells

In mutant cells characterized by an accumulation of the precursor p65-kDa (W18C, E309K, I325F and G389A) or of NOX2 in intracellular compartments (H338Y, P339H), we analysed the location of both proteins by conducting a co-staining experiment and confocal microscopy using antibodies directed against calnexin, an endoplasmic reticulum marker , GM130, a Golgi apparatus marker and lamin B1, a nuclear membrane marker. We used the 54.1 monoclonal antibody, which can recognize both p65-kDa and NOX2.

In the Mock-X^0CGD PLB-985 cells, no NOX2 was expressed, but calnexin delimited the endoplasmic reticulum (Figure 4A). In WT-NOX2 PLB-985 cells, NOX2 was mainly localized at the plasma membrane (Figure 4A) and there was no colocalization of NOX2 and calnexin, as suggested by the absence of overlapping between the clouds of green (NOX2 or p65-kDa) and red (calnexin fluorescence (open angle in both clouds) assessed by the Leica Instruments colocalization software (Figure 4B). In the H101Y mutant considered as an X^0-CGD phenotype (no NOX2 expression and no

oxidase activity), the 54.1 antibody revealed the presence of the precursor p65-kDa that accumulates in the ER or in compartments close to it because of a yellow fluorescence of the merge (Figure 4A). Colocalization was evidenced in some cells, as seen in Figure 4B. In the group A mutants with an abnormal p65/NOX2 ratio (W18C, E309K and I325F), a yellow merge was seen inside the cells, as in the H101Y mutant (Figure 4A). Using the colocalization program, we showed that part of the cells coexpressed p65-KDa and calnexin in the ER (yellow cells in the quarter). In addition, both green (p65-kDa) and red (calnexin) clouds moved closer (more closed angle in both clouds) compared to the WT-NOX2 cells. As we demonstrated above, the H338Y and P339H mutants are characterized by a normal p65/NOX2 ratio (i.e., no accumulation of the p65-kDa precursor in subcellular compartments); the co-location of NOX2/p65-kDa with the ER was less evident than for the previous mutants (Figure 4B). In addition, as in the WT-NOX2 PLB-985 cells, a green fluorescence can be clearly seen over the yellow merge, suggesting NOX2 expression at the plasma membrane (Figure 4A). Finally, for the G189A mutant, p65-kDa is mainly in intracellular compartments, and the analysis of the colocalization is difficult because of the very low expression of NOX2 and p65-KDa.
Neither NOX2 nor p65-kDa colocalizes with the Golgi apparatus or the nuclear membrane in the mutants analyzed (Supplementary Figures S1 and S2).

Study of the interaction between the precursor p65-kDa and p22^{phox} in X^{-}CGD PLB-985 mutants with an abnormal p65/NOX2 ratio

In order to determine if the defective synthesis of cytb_{558} in the mutants with an abnormal accumulation of the p65-kDa precursor in intracellular compartments was caused by faulty p22^{phox} and p65-kDa assembly, we performed co-immunoprecipitation experiments from X^{-}-CGD mutant cells. The same amount of proteins (100 µg) in each lane was analysed using SDS-PAGE and Western blot. Following immunoprecipitation of membrane proteins with CS9 (an antibody against p22^{phox}) in the MACS column, the p65/p22^{phox} complex was eluted by the SDS-PAGE sample buffer (positive fraction) in the case of the WT NOX2 PLB-985 cells (Figure 5). However, the surplus of the p65/p22^{phox} complex was recovered in the flow-through (negative fraction). Indeed, we adapted the quantity of CS9 antibody against p22^{phox} to trap the amount of p65-kDa of the mutants but this quantity may not be sufficient to trap the p65-kDa/p22^{phox} complex of the WT-NOX2 PLB-985 cells. IgG1 antibodies as irrelevant antibodies demonstrated the specificity of the co-immunoprecipitation in WT NOX2 PLB-985 cells. We also analyzed the mutant H101Y PLB-985 cell lines as a control as follows. The H101Y mutation is assumed to disturb cytb_{558} synthesis because it impairs heme incorporation in NOX2 leading to a lack of p65-kDa and p22^{phox} binding, as demonstrated previously (13). Indeed, we found a total dissociation of p65-kDa, eluted in the unbound fraction, whereas p22^{phox} was eluted with the SDS-PAGE sample buffer (Figure 5). In the group A X^{-}-CGD mutants and in the G389A mutant, the totality of p65-kDa was eluted in the flow-through fraction, whereas most of the p22^{phox} was eluted with the sample buffer for SDS-PAGE. We conclude that the W18C, H101Y, E309K, I325F, and G389A mutations prevent p65/p22^{phox} binding. For group B mutants (H338Y, P339H), whereas some p65-kDa is eluted directly in the flow-through, probably because of a nonspecific effect of detergent treatment (1% Triton X100). In addition, we cannot exclude that part of p65-kDa may be unbound in the cells. However, part of the precursor p65-kDa is eluted with p22^{phox} in the positive fraction (SDS-PAGE sample buffer). Thus the defect of cytb_{558} synthesis in the H338Y and P339H mutants probably stems from another cause than a defect of p65-kDa/p22^{phox} binding. This point will be discussed further.

DISCUSSION

We successfully reproduced the majority of the X^{-}-CGD cases in the PLB-985 cell model. Surprisingly, we observed that in most X^{-}-CGD PLB-985 cells, NOX2 expression at the plasma membrane, as measured by flow cytometry, decreases after differentiation. We suggest that the increase of p22^{phox} during the differentiation step (data not shown) could lead to controlled expression and trafficking of the recombinant mutated NOX2 protein that is continuously produced in transfected PLB-985 cells. We should point out that all the results described here were obtained using

differentiated mutated PLB-985 cells. The first point was that all the X^{-}-CGD mutations did not alter the transcription step, as suggested by the equivalent level of NOX2 mRNA analysed by RT-PCR.
Among the ten X^{-}-CGD mutations reproduced in the PLB-985 cell line, one mutation **I187_I189del** was considered as having an X^{0}CGD profile because no expression of NOX2 and no NADPH oxidase activity could be measured. However, this mutation was only listed as an X^{-}-CGD case in a review without any results supporting this phenotype (33). The **I187_I189del** is in the IVth transmembrane region of NOX2 closed to the D-loop. The D-loop of NOX2 was demonstrated to be involved in the control of NADPH oxidase activity (42) (52). In addition, a new role for the D-loop of NOX4 in folding and interaction with p22^{phox} has been proposed (17). Thus I187–I189 residues are in an important functional and structural region of NOX2. The cell model of the **H101Y** mutation also leads to an X^{0}CGD profile, like the I187_I189del mutation, whereas Tsuda et al. described 8% NOX2 (24). However, in the figure of the Western blot in his article we did not see any NOX2 band. This highly conserved histidine in NOX1–4, is one of the four involved in the coordination of hemes in cytb_{558}, described as an essential step for the assembly of NOX2 with p22^{phox} (13). Thus, the defect of heme incorporation in H101Y mutant cells affects cytb_{558} synthesis by blocking the association between the precursor p65-kDa and p22^{phox} in ER compartments. Indeed in our work, this mutant served as a useful control of the dissociation of the two proteins in co-immunoprecipitation experiments and to visualize the accumulation of p65-kDa in the ER or in nearby compartments using confocal microscopy.

Then according to the NOX2 expression and the NADPH oxidase activity, we classified the X^{-}-CGD mutants into two groups. Group B mutants **H338Y, P339H, G389A, and F565_F570del,** lead to the same phenotype in PLB-985 cells; a discrepancy between NOX2 expression at the plasma membrane as measured by flow cytometry (4–12%) and the complete absence of NADPH oxidase activity. This phenotype was previously reported in human neutrophils (36) and confirms the robustness of our approach. These X^{-}-CGD mutations affect not only the structure of NOX2, but also its activity. Both H338 and P339 residues are located in the binding site for the FAD isoalloxazine ring (Figure 6A) [43]. FAD depletion in the neutrophils from a patient exhibiting the H338Y mutation has been previously reported (36). The absence of FAD could explain the absence of NADPH oxidase activity in these mutants as previously demonstrated [43]. In addition, both mutations do not affect p65/p22^{phox} binding. Thus both H338Y and P339H mutations contribute to disturbing the catalytic site of NOX2 (Figure 6A). Surprisingly, in the H338Y and P339H mutants, NOX2 was found in both the plasma membrane and the intracellular compartments. This was previously shown for the H338Y mutation only [37,38]. It is possible that both mutations lead to partial structural deformation of the cytb_{558} such that it cannot be optimally incorporated into the plasma membrane and accumulates inside the cells in undefined compartments different from ER.
The **F565_F570del mutation** originally reported in the X^{-}-CGD patient's neutrophils (22) belongs to the group B mutants like the previous ones. In competition experiments using peptides, the carboxy terminus of NOX2 has been shown to be directly or indirectly involved in p47^{phox} subunit binding (53,54). Then using directed mutagenesis of the last 11 residues of NOX2, Zhen et al. demonstrated that this region plays a structural role rather than a functional one (55). In addition, the F570 is highly conserved in the FAD binding in the proteins of the ferredoxin reductase family and is involved in the stabilization of the isoalloxazine ring of the FAD [43]. Indeed, our present work demonstrates that the last six residues of NOX2, highly conserved in the NOX1–4 proteins, play both structural and functional roles. In addition, the cytb_{558} synthesis defect in this mutant is due to an intrinsic instability of the mature NOX2 protein rather than a defect in its maturation process itself. The absence of p65-kDa accumulation in intracellular compartments for this mutant consolidates this conclusion.
The effect of the **G389A** mutation in the cytb_{558} synthesis process is intriguing. This glycine is highly conserved in NOX1–4 and is located in a highly conserved region ^{388}DGPFG^{392}. Through sequence analogy with the ferredoxin reductase family, we found a match with sequences conserved in the FAD binding pocket (http://www.ebi.ac.uk/interpro/sequencesearch/iprscan5-R20140418-130743-0988-23575230-pg). Like the previous group B mutants, the NADPH oxidase is null, but unlike the others, a substantial accumulation of the precursor p65-kDa demonstrated a blockage in the maturation process of cytb_{558} due to a defect in p65-kDa and p22^{phox} binding. Other cases of X^{0}-CGD originate from Gly 389 mutations – G389R, G389V and G389E – were reported that underlie the importance of this residue (19). From its location in the dehydrogenase domain (Figure 6B), at the interface with the transmembrane part of the protein, Gly 389 is not in a position where it can be a direct contributor to

the interaction with p22^{phox}. However, the presence of a glycine, without any bulky side chain, seems to be essential to ensure the structural integrity required for p22^{phox} binding. In addition, this Gly is essential to maintain the electron transfer inside NOX2, possibly by preserving the integrity of the coupling between the FAD of the dehydrogenase domain and the heme moieties within the membranous domain.

Finally, in the following group A mutants – **W18C, E309K, K315del and I325F –** NOX2 expression is directly proportional to the NADPH oxidase activity; therefore, these mutations affect NOX2 synthesis and stability only. We observed a high p65/NOX2 ratio caused by the abnormal accumulation of the p65-kDa precursor in structures close to the ER or in the ER itself in all but K315del. This deletion affects the stability of NOX2 only. As for the G389A mutant, the accumulation of the p65-kDa precursor is explained by a defect in binding with p22^{phox}, as demonstrated by the co-immunoprecipitation experiment. It remains uncertain as to whether these residues are directly or indirectly involved in p22^{phox} binding. **W18C** is one of two missense mutations of XCGD found in the first potential transmembrane passage of NOX2, whose role has not yet been determined (19). W18 is conserved in NOX1, NOX3 and NOX4 (but not in NOX5) for which a connection with p22^{phox} is necessary for their activity. Therefore, the first transmembrane passage of NOX2 and particularly W18 could potentially be directly involved in the binding of p22^{phox}. **I325** and **G389** residues are located in the same region of the FAD-binding domain, at the interface between the dehydrogenase and the transmembrane domain (Figure 6B). Mutations in these positions introducing some bulkier residues may induce a packing problem at this interface between both domains of the NOX2 protein. The fact that it abrogates p65/p22^{phox} binding suggests that the p22^{phox} binding site is spread over both regions, the transmembrane region and the dehydrogenase domain, that need to be well oriented to provide an extended and functional interaction interface for p22^{phox} (red circle in Figure 6B). Nonetheless, these residues are also postulated as being close from the surface and considering the size of some substitution in X^{-}-CGD mutants (like in I325F), a direct perturbance of a surface interaction site could also be postulated (Figure 6B). Thus, these mutations could impact either directly or indirectly on p22^{phox} binding interface. The role played by the **E309** residue could be quite different. Although the E309K mutation prevented p65/p22^{phox} binding (as I325F and G389A mutations), E309 is likely to be exposed on the dehydrogenase domain surface (Figure 6B). Indeed this mutation of a charged amino acid side chain oriented toward the solvent is not expected to disorganize domain orientations. Its deleterious effect and the fact that it is strictly conserved from NOX1–4 support the notion that it could plays a direct role in the interaction with p22^{phox}.

In conclusion we increased the understanding of the impact of these mutations on the process of cytb_{558} synthesis, previously restricted by insufficient biological material. In the absence of a NOX2/p22^{phox} structure, the analysis of the X^{-}-CGD mutants reported herein provides the first indications on the structural requirement and potential NOX2 regions required for p22^{phox} interaction, spread over the entire NOX2 structure, like the first transmembrane passage (W18), the intermediate region between the membrane and the cytosolic dehydrogenase domains of NOX2 (E309, I325, G389) and a surface docking site on the dehydrogenase domain located with the E309K mutation. In addition, this study has demonstrated that FAD-binding pocket integrity is closely related to NOX2 stability [H338, P339, G389 and 570_570del].

AUTHOR CONTRIBUTION

Sylvain Beaumel undertook the experiments in Figures 2-5; Didier Grunwald performed the confocal microscopy analysis and took photos from the slides prepared by Sylvain Beaumel. Marie José Stasia designed the experiments, analysed the experimental data and wrote the paper. Franck Fieschi analysed the data, wrote part of the discussion and prepared the Figure 6.

ACKNOWLEDGEMENTS

The coordinates of the model of the C-terminal domain of NOX2 were kindly provided by Profs. A. Segal and W.R. Taylor. The authors are grateful to Prof. Mary C. Dinauer for the generous gift of X^0-CGD PLB-985 cells. We are very grateful to Cécile Martel, Michelle Mollin, Julie Brault, Charlotte Genestet and Erwan Goutagny for their enthusiasm in their work at the CDiReC. Special thanks are extended to Lila Laval for her excellent secretarial work and to Linda Northrup for editing the manuscript.

FUNDING

MJS is grateful for support from the CGD Research Trust grant award reference J4G/09/09, the University Joseph Fourier Grenoble - Alpes (AGIR program 2013), the Faculty of Medicine; the Ministry of Education and Research, MENRT and the Regional Clinical Research Department, DRCI, Grenoble University Hospital. FF thanks the Institut Universitaire de France for financial support and the ANR program for the grant 2010-1536-01 “prototype NOX”.

REFERENCES

1. Dale, D. C., Boxer, L., and Liles, W. C. (2008) The phagocytes: neutrophils and monocytes. *Blood* **112**, 935-945
2. van den Berg, J. M., van Koppen, E., Ahlin, A., Belohradsky, B. H., Bernatowska, E., Corbeel, L., Espanol, T., Fischer, A., Kurenko-Deptuch, M., Mouy, R., Petropoulou, T., Roesler, J., Seger, R., Stasia, M. J., Valerius, N. H., Weening, R. S., Wolach, B., Roos, D., and Kuijpers, T. W. (2009) Chronic granulomatous disease: the European experience. *PLoS One* **4**, e5234
3. Vignais, P. V. (2002) The superoxide-generating NADPH oxidase: structural aspects and activation mechanism. *Cell Mol Life Sci* **59**, 1428-1459
4. Henderson, L. M. (1998) Role of histidines identified by mutagenesis in the NADPH oxidase-associated H+ channel. *J Biol Chem* **273**, 33216-33223
5. Bedard, K., and Krause, K. H. (2007) The NOX family of ROS-generating NADPH oxidases: physiology and pathophysiology. *Physiol Rev* **87**, 245-313
6. Kawahara, T., Quinn, M. T., and Lambeth, J. D. (2007) Molecular evolution of the reactive oxygen-generating NADPH oxidase (Nox/Duox) family of enzymes. *BMC Evol Biol* **7**, 109
7. Paclet, M. H., Henderson, L. M., Campion, Y., Morel, F., and Dagher, M. C. (2004) Localization of Nox2 N-terminus using polyclonal antipeptide antibodies. *Biochem J* **382**, 981-986
8. Biberstine-Kinkade, K. J., DeLeo, F. R., Epstein, R. I., LeRoy, B. A., Nauseef, W. M., and Dinauer, M. C. (2001) Heme-ligating histidines in flavocytochrome b(558): identification of specific histidines in gp91(phox). *J Biol Chem* **276**, 31105-31112
9. Wallach, T. M., and Segal, A. W. (1997) Analysis of glycosylation sites on gp91phox, the flavocytochrome of the NADPH oxidase, by site-directed mutagenesis and translation in vitro. *Biochem J* **321 (Pt 3)**, 583-585
10. Yu, L., Zhen, L., and Dinauer, M. C. (1997) Biosynthesis of the phagocyte NADPH oxidase cytochrome b558. Role of heme incorporation and heterodimer formation in maturation and stability of gp91phox and p22phox subunits. *J Biol Chem* **272**, 27288-27294
11. Yu, L., Quinn, M. T., Cross, A. R., and Dinauer, M. C. (1998) Gp91(phox) is the heme binding subunit of the superoxide-generating NADPH oxidase. *Proc Natl Acad Sci U S A* **95**, 7993-7998
12. Yu, L., DeLeo, F. R., Biberstine-Kinkade, K. J., Renee, J., Nauseef, W. M., and Dinauer, M. C. (1999) Biosynthesis of flavocytochrome b558 . gp91(phox) is synthesized as a 65-kDa precursor (p65) in the endoplasmic reticulum. *J Biol Chem* **274**, 4364-4369
13. DeLeo, F. R., Burritt, J. B., Yu, L., Jesaitis, A. J., Dinauer, M. C., and Nauseef, W. M. (2000) Processing and maturation of flavocytochrome b558 include incorporation of heme as a prerequisite for heterodimer assembly. *J Biol Chem* **275**, 13986-13993
14. Kawahara, T., Ritsick, D., Cheng, G., and Lambeth, J. D. (2005) Point mutations in the proline-rich region of p22phox are dominant inhibitors of Nox1- and Nox2-dependent reactive oxygen generation. *J Biol Chem* **280**, 31859-31869
15. Zhu, Y., Marchal, C. C., Casbon, A. J., Stull, N., von Lohneysen, K., Knaus, U. G., Jesaitis, A. J., McCormick, S., Nauseef, W. M., and Dinauer, M. C. (2006) Deletion mutagenesis of p22phox subunit of flavocytochrome b558: identification of regions critical for gp91phox maturation and NADPH oxidase activity. *J Biol Chem* **281**, 30336-30346

16. von Lohneysen, K., Noack, D., Jesaitis, A. J., Dinauer, M. C., and Knaus, U. G. (2008) Mutational analysis reveals distinct features of the Nox4-p22 phox complex. *J Biol Chem* **283**, 35273-35282
17. von Lohneysen, K., Noack, D., Wood, M. R., Friedman, J. S., and Knaus, U. G. (2010) Structural insights into Nox4 and Nox2: motifs involved in function and cellular localization. *Mol Cell Biol* **30**, 961-975
18. Stasia, M. J., and Li, X. J. (2008) Genetics and immunopathology of chronic granulomatous disease. *Semin Immunopathol* **30**, 209-235
19. Roos, D., Kuhns, D. B., Maddalena, A., Roesler, J., Lopez, J. A., Ariga, T., Avcin, T., de Boer, M., Bustamante, J., Condino-Neto, A., Di Matteo, G., He, J., Hill, H. R., Holland, S. M., Kannengiesser, C., Koker, M. Y., Kondratenko, I., van Leeuwen, K., Malech, H. L., Marodi, L., Nunoi, H., Stasia, M. J., Ventura, A. M., Witwer, C. T., Wolach, B., and Gallin, J. I. (2010) Hematologically important mutations: X-linked chronic granulomatous disease (third update). *Blood Cells Mol Dis*
20. Bolscher, B. G., de Boer, M., de Klein, A., Weening, R. S., and Roos, D. (1991) Point mutations in the beta-subunit of cytochrome b558 leading to X-linked chronic granulomatous disease. *Blood* **77**, 2482-2487
21. Roos, D., de Boer, M., Borregard, N., Bjerrum, O. W., Valerius, N. H., Seger, R. A., Muhlebach, T., Belohradsky, B. H., and Weening, R. S. (1992) Chronic granulomatous disease with partial deficiency of cytochrome b558 and incomplete respiratory burst: variants of the X-linked, cytochrome b558-negative form of the disease. *J Leukoc Biol* **51**, 164-171
22. Bu-Ghanim, H. N., Segal, A. W., Keep, N. H., and Casimir, C. M. (1995) Molecular analysis in three cases of X91- variant chronic granulomatous disease. *Blood* **86**, 3575-3582
23. Porter, C. D., Kuribayashi, F., Parkar, M. H., Roos, D., and Kinnon, C. (1996) Detection of gp91-phox precursor protein in B-cell lines from patients with X-linked chronic granulomatous disease as an indicator for mutations impairing cytochrome b558 biosynthesis. *Biochem J* **315 (Pt 2)**, 571-575
24. Tsuda, M., Kaneda, M., Sakiyama, T., Inana, I., Owada, M., Kiryu, C., Shiraishi, T., and Kakinuma, K. (1998) A novel mutation at a probable heme-binding ligand in neutrophil cytochrome b558 in atypical X-linked chronic granulomatous disease. *Hum Genet* **103**, 377-381
25. Kaneda, M., Sakuraba, H., Ohtake, A., Nishida, A., Kiryu, C., and Kakinuma, K. (1999) Missense mutations in the gp91-phox gene encoding cytochrome b558 in patients with cytochrome b positive and negative X-linked chronic granulomatous disease. *Blood* **93**, 2098-2104
26. Roesler, J., Heyden, S., Burdelski, M., Schafer, H., Kreth, H. W., Lehmann, R., Paul, D., Marzahn, J., Gahr, M., and Rosen-Wolff, A. (1999) Uncommon missense and splice mutations and resulting biochemical phenotypes in German patients with X-linked chronic granulomatous disease. *Exp Hematol* **27**, 505-511
27. Stasia, M. J., Bordigoni, P., Floret, D., Brion, J. P., Bost-Bru, C., Michel, G., Gatel, P., Durant-Vital, D., Voelckel, M. A., Li, X. J., Guillot, M., Maquet, E., Martel, C., and Morel, F. (2005) Characterization of six novel mutations in the CYBB gene leading to different sub-types of X-linked chronic granulomatous disease. *Hum Genet* **116**, 72-82
28. von Goessel, H., Hossle, J. P., Seger, R., and Gungor, T. (2006) Characterization of 17 new cases of X-linked chronic granulomatous disease with seven novel mutations in the CYBB gene. *Exp Hematol* **34**, 528-535
29. Martel, C., Mollin, M., Beaumel, S., Brion, J. P., Coutton, C., Satre, V., Vieville, G., Callanan, M., Lefebvre, C., Salmon, A., Pagnier, A., Plantaz, D., Bost-Bru, C.,

Eitenschenck, L., Durieu, I., Floret, D., Galambrun, C., Chambost, H., Michel, G., Stephan, J. L., Hermine, O., Blanche, S., Blot, N., Rubie, H., Pouessel, G., Drillon-Haus, S., Conrad, B., Posfay-Barbe, K. M., Havlicekova, Z., Voskresenky-Baricic, T., Jadranka, K., Arriazu, M. C., Garcia, L. A., Sfaihi, L., Bordigoni, P., and Stasia, M. J. (2012) Clinical, functional and genetic analysis of twenty-four patients with chronic granulomatous disease - identification of eight novel mutations in CYBB and NCF2 genes. *J Clin Immunol* **32**, 942-958

30. Rae, J., Newburger, P. E., Dinauer, M. C., Noack, D., Hopkins, P. J., Kuruto, R., and Curnutte, J. T. (1998) X-Linked chronic granulomatous disease: mutations in the CYBB gene encoding the gp91-phox component of respiratory-burst oxidase. *Am J Hum Genet* **62**, 1320-1331
31. Patino, P. J., Perez, J. E., Lopez, J. A., Condino-Neto, A., Grumach, A. S., Botero, J. H., Curnutte, J. T., and Garcia de Olarte, D. (1999) Molecular analysis of chronic granulomatous disease caused by defects in gp91-phox. *Hum Mutat* **13**, 29-37
32. Ishibashi, F., Nunoi, H., Endo, F., Matsuda, I., and Kanegasaki, S. (2000) Statistical and mutational analysis of chronic granulomatous disease in Japan with special reference to gp91-phox and p22-phox deficiency. *Hum Genet* **106**, 473-481
33. Heyworth, P. G., Curnutte, J. T., Rae, J., Noack, D., Roos, D., van Koppen, E., and Cross, A. R. (2001) Hematologically important mutations: X-linked chronic granulomatous disease (second update). *Blood Cells Mol Dis* **27**, 16-26
34. Vihinen, M., Arredondo-Vega, F. X., Casanova, J. L., Etzioni, A., Giliani, S., Hammarstrom, L., Hershfield, M. S., Heyworth, P. G., Hsu, A. P., Lahdesmaki, A., Lappalainen, I., Notarangelo, L. D., Puck, J. M., Reith, W., Roos, D., Schumacher, R. F., Schwarz, K., Vezzoni, P., Villa, A., Valiaho, J., and Smith, C. I. (2001) Primary immunodeficiency mutation databases. *Adv Genet* **43**, 103-188
35. Di Matteo, G., Giordani, L., Finocchi, A., Ventura, A., Chiriaco, M., Blancato, J., Sinibaldi, C., Plebani, A., Soresina, A., Pignata, C., Dellepiane, R. M., Trizzino, A., Cossu, F., Rondelli, R., Rossi, P., De Mattia, D., and Martire, B. (2009) Molecular characterization of a large cohort of patients with Chronic Granulomatous Disease and identification of novel CYBB mutations: an Italian multicenter study. *Mol Immunol* **46**, 1935-1941
36. Yoshida, L. S., Saruta, F., Yoshikawa, K., Tatsuzawa, O., and Tsunawaki, S. (1998) Mutation at histidine 338 of gp91(phox) depletes FAD and affects expression of cytochrome b558 of the human NADPH oxidase. *J Biol Chem* **273**, 27879-27886
37. Lin, S. J., Huang, Y. F., Chen, J. Y., Heyworth, P. G., Noack, D., Wang, J. Y., Lin, C. Y., Chiang, B. L., Yang, C. M., Liu, C. C., and Shieh, C. C. (2002) Molecular quality control machinery contributes to the leukocyte NADPH oxidase deficiency in chronic granulomatous disease. *Biochim Biophys Acta* **1586**, 275-286
38. Huang, Y. F., Liu, S. Y., Yen, C. L., Yang, P. W., and Shieh, C. C. (2009) Thapsigargin and flavin adenine dinucleotide ex vivo treatment rescues trafficking-defective gp91phox in chronic granulomatous disease leukocytes. *Free Radic Biol Med* **47**, 932-940
39. Stasia, M. J., Lardy, B., Maturana, A., Rousseau, P., Martel, C., Bordigoni, P., Demaurex, N., and Morel, F. (2002) Molecular and functional characterization of a new X-linked chronic granulomatous disease variant (X91+) case with a double missense mutation in the cytosolic gp91phox C-terminal tail. *Biochim Biophys Acta* **1586**, 316-330
40. Zhen, L., King, A. A., Xiao, Y., Chanock, S. J., Orkin, S. H., and Dinauer, M. C. (1993) Gene targeting of X chromosome-linked chronic granulomatous disease locus

in a human myeloid leukemia cell line and rescue by expression of recombinant gp91phox. *Proc Natl Acad Sci U S A* **90**, 9832-9836
41. Tucker, K. A., Lilly, M. B., Heck, L., Jr., and Rado, T. A. (1987) Characterization of a new human diploid myeloid leukemia cell line (PLB-985) with granulocytic and monocytic differentiating capacity. *Blood* **70**, 372-378
42. Li, X. J., Grunwald, D., Mathieu, J., Morel, F., and Stasia, M. J. (2005) Crucial role of two potential cytosolic regions of Nox2, 191TSSTKTIRRS200 and 484DESQANHFAVHHDEEKD500, on NADPH oxidase activation. *J Biol Chem* **280**, 14962-14973
43. Towbin, H., Staehelin, T., and Gordon, J. (1979) Electrophoretic transfer of proteins from polyacrylamide gels to nitrocellulose sheets: procedure and some applications. *Proc Natl Acad Sci U S A* **76**, 4350-4354
44. Laemmli, U. K. (1970) Cleavage of structural proteins during the assembly of the head of bacteriophage T4. *Nature* **227**, 680-685
45. Burritt, J. B., Fritel, G. N., Dahan, I., Pick, E., Roos, D., and Jesaitis, A. J. (2000) Epitope identification for human neutrophil flavocytochrome b monoclonals 48 and 449. *Eur J Haematol* **65**, 407-413
46. Baniulis, D., Nakano, Y., Nauseef, W. M., Banfi, B., Cheng, G., Lambeth, D. J., Burritt, J. B., Taylor, R. M., and Jesaitis, A. J. (2005) Evaluation of two anti-gp91phox antibodies as immunoprobes for Nox family proteins: mAb 54.1 recognizes recombinant full-length Nox2, Nox3 and the C-terminal domains of Nox1-4 and cross-reacts with GRP 58. *Biochim Biophys Acta* **1752**, 186-196
47. Debeurme, F., Picciocchi, A., Dagher, M. C., Grunwald, D., Beaumel, S., Fieschi, F., and Stasia, M. J. (2010) Regulation of NADPH oxidase activity in phagocytes: relationship between FAD/NADPH binding and oxidase complex assembly. *J Biol Chem* **285**, 33197-33208
48. Smith, P. K., Krohn, R. I., Hermanson, G. T., Mallia, A. K., Gartner, F. H., Provenzano, M. D., Fujimoto, E. K., Goeke, N. M., Olson, B. J., and Klenk, D. C. (1985) Measurement of protein using bicinchoninic acid. *Anal Biochem* **150**, 76-85
49. Chomczynski, P., and Sacchi, N. (1987) Single-step method of RNA isolation by acid guanidinium thiocyanate-phenol-chloroform extraction. *Anal Biochem* **162**, 156-159
50. Trocme, C., Gaudin, P., Berthier, S., Barro, C., Zaoui, P., and Morel, F. (1998) Human B lymphocytes synthesize the 92-kDa gelatinase, matrix metalloproteinase-9. *J Biol Chem* **273**, 20677-20684
51. Bail, S., Swerdel, M., Liu, H., Jiao, X., Goff, L. A., Hart, R. P., and Kiledjian, M. (2010) Differential regulation of microRNA stability. *Rna* **16**, 1032-1039
52. Carrichon, L., Picciocchi, A., Debeurme, F., Defendi, F., Beaumel, S., Jesaitis, A. J., Dagher, M. C., and Stasia, M. J. (2012) Characterization of superoxide overproduction by the D-Loop(Nox4)-Nox2 cytochrome b(558) in phagocytes-Differential sensitivity to calcium and phosphorylation events. *Biochim Biophys Acta*
53. Kleinberg, M. E., Mital, D., Rotrosen, D., and Malech, H. L. (1992) Characterization of a phagocyte cytochrome b558 91-kilodalton subunit functional domain: identification of peptide sequence and amino acids essential for activity. *Biochemistry* **31**, 2686-2690
54. Uhlinger, D. J., Tyagi, S. R., and Lambeth, J. D. (1995) On the mechanism of inhibition of the neutrophil respiratory burst oxidase by a peptide from the C-terminus of the large subunit of cytochrome b558. *Biochemistry* **34**, 524-527
55. Zhen, L., Yu, L., and Dinauer, M. C. (1998) Probing the role of the carboxyl terminus of the gp91phox subunit of neutrophil flavocytochrome b558 using site-directed mutagenesis. *J Biol Chem* **273**, 6575-6581

Table 1 Expression of NOX2, p65-kDa and NADPH oxidase activity in the X$^-$-CGD transfected PLB-985 cells

The relative level of recombinant NOX2 (and p65-kDa) was measured after PLB-985 cell differentiation with 0.5% DMF for 6 days. NOX2 expression measured by flow cytometry was calculated using G mean fluorescence of each PLB 985 cell line. NOX2 and p65-KDa expression were also estimated by Western blot based on scanning densitometry of immunoblots performed with the 48 monoclonal antibodies (GelDoc® BioRad system). ROS production was measured by luminol-amplified chemiluminescence in 5.10^5 differentiated and transfected X$^-$-CGD PLB-985 cells after PMA stimulation. Results are represented as total activity by the sum of relative luminescence units measured in 60 min at 37°C. Percentages were calculated from the values of the control WT NOX2 PLB-985 cells. Data are the mean ± SD of (n) range experiments. In group A mutants, the level of NOX2 expressed at the plasma membrane measured by flow cytometry is directly proportional to the level of NADPH oxidase activity. In group B mutants, the NOX2 expression at the plasma membrane was variable, whereas the NADPH oxidase activity was totally abolished. Values of NOX2 expression measured by flow cytometry and NADPH oxidase activity for mutants A and B are in bold.

		FLOW CYTOMETRY NOX2		**WESTERN BLOT (n = 3) NOX2**	**p65-kDa**		**CHEMILUMINESCENCE H_2O_2 PRODUCTION**		
		G mean	% of control	% of control	% of control	ratio p65/NOX2	Sum RLU x 10^3		% of control
	WT NOX2 (control)	123.0 ± 28	(n=10)	100	100	100	1	10,122 ± 1,215	(n=10)	100
	Mock X-CGD	2.9 ± 0.7	(n=10)	0	0	0	/	14 ± 9	(n=10)	0
Group A	**W18C**	24.0 ± 5.0	(n=10)	**17**	12.1 ± 2.8	59.1 ± 19.6	5	**2,034 ± 446**	**(n=10)**	**20**
Group A	**P56L**	6.3 ± 3.9	(n=10)	**3**	1.0 ± 0.8	50.3 ± 19.3	50	597 ± 233	(n=10)	**6**
Group A	**E309K**	8.1 ± 3.6	(n=10)	**4**	8.2 ± 2.1	48.3 ± 17.7	6	415 ± 243	(n=10)	**4**
Group A	**K315del**	13.0 ± 4.8	(n=10)	**8**	11.0 ± 1.8	11.5 ± 1.3	1	891 ± 314	(n=10)	**9**
Group A	**I325F**	4.6 ± 2.4	(n=10)	**2**	1.5 ± 0.6	26.8 ± 6.6	18	423 ± 139	(n=10)	**4**
Group B	**H338Y**	14.4 ± 2.8	(n=5)	**10**	46.4 ± 16.3	56.6 ± 16.4	1	11 ± 6	(n=5)	**0**
Group B	**P339H**	8.7 ± 2.4	(n=5)	**5**	38.0 ± 17.1	36.7 ± 15.3	1	9 ± 5	(n=5)	**0**
Group B	**G389A**	4.4 ± 2.5	(n=5)	**2**	0.8 ± 0.8	21.5 ± 4.5	27	7 ± 4	(n=5)	**0**
Group B	**F565_F570del**	18.5 ± 7.0	(n=5)	**12**	16.3 ± 8.1	16.0 ± 5.0	1	18 ± 7	(n=5)	**0**
X^0 CGD	H101Y	2.6 ± 0.6	(n=5)	0	0	71.7 ± 10.0	/	10 ± 2	(n=5)	0
X^0 CGD	A156T	2.5 ± 0.4	(n=5)	0	0	36.0 ± 9.2	/	32 ± 11	(n=5)	0
X^0 CGD	I187_I189del	2.6 ± 0.8	(n=5)	0	0	19.3 ± 5.9	/	30 ± 12	(n=5)	0
X^0 CGD	C244S	2.6 ± 0.5	(n=5)	0	0	3.0 ± 2.0	/	30 ± 11	(n=5)	0
X^0 CGD	C244Y	2.5 ± 0.7	(n=5)	0	0	38.7 ± 6.0	/	16 ± 6	(n=5)	0
X^0 CGD	V534_G538del	2.6 ± 0.9	(n=5)	0	0	6.3 ± 2.1	/	10 ± 4	(n=5)	0

FIGURE LEGENDS

Figure 1 Location in NOX2 and conservation among NOX family members of amino acids involved in X$^-$-CGD mutations.
(A) Glycosylated asparagines are located in the external loops of NOX2 and numbered by their residue numbers. The four heme-binding histidines located in the third and fifth transmembrane domains are shown by single-letter code as H. The potential FAD- and NADPH-binding domains are illustrated by dotted boxes. The X$^-$-CGD mutations studied in the article are in red and other mutations causing X$^-$-CGD are in blue (Roos et al. 2010). These mutations are present in the whole sequence, whereas four clusters can be delimitated by the high frequency of the location of X$^-$-CGD mutations as red circles; the intracytosolic D-loop, the potential FAD-binding sites, the C-terminal region and a region between the sixth transmembrane passage and the FAD-binding site. (**B)** The X$^-$-CGD mutations studied in this work (in red) are totally preserved among NOX1–4. The potential binding sites of NADPH and FAD are in pink and orange, respectively, the histidines that coordinate hemes are in green and the glycosylated asparagines are in blue. The alignments were done using the website http://www.ebi.ac.uk/Tools/msa/clustalw2/.

Figure 2: RT-PCR and quantitative PCR analysis of the mRNA of the transfected X$^-$-CGD PLB-985 cells. (A) RT-PCR was performed on total RNA extracts with primers specific for p22^{phox} or NOX2 cDNA. As a control for RNA quality and equal loading, RT-PCR was performed with primers for geneticin. The results are representative of three independent experiments. (B) Real-time PCR was performed as described in Materials and Methods. Results are expressed as means of the ratio from four different qPCR performed from two different RT-PCR from one total RNA extraction for each type of differentiated cell. Data are the mean ± SD of four independent experiments.

Figure 3 Analysis of mutated NOX2 expression in transfected X$^-$-CGD PLB-985 cells by flow cytometry and Western blot
(**A**) Flow cytometry analysis of NOX2 expression in undifferentiated (UD) and differentiated (D) transfected X$^-$-CGD PLB-985 cells. (5.10^5) cells were incubated with the NOX2 monoclonal antibody 7D5 and then with a phycoerythrin-labelled goat-F(ab′)$_2$ fragment anti-mouse IgG as described in Material and Methods. The mouse IgG1 isotype was used as an irrelevant monoclonal antibody. In Mock X^0-CGD PLB-985 cells there is no NOX2 expression (dotted line) after WT NOX2 cDNA transfection; NOX2 is stably expressed in the WT NOX2 PLB985 cells (white histogram). A diminished NOX2 expression is visible in the X$^-$-CGD PLB-985 cells (grey histogram). The same observations were obtained in at least four independent experiments. **(B)** Immunoblot analysis of NOX2, p22^{phox} and the precursor of NOX2 p65-kDa was performed on 1% Triton X-100 soluble extracts (100 µg) from X$^-$-CGD PLB-985 cells, subjected to SDS-PAGE, blotted onto a nitrocellulose sheet and revealed with monoclonal antibodies 48 and 449, respectively. P47^{phox} monoclonal antibody served as a loading control. Western blots of undifferentiated and differentiated PLB-985 cells have unequal times of exposure.

Figure 4 NOX2 and/or p65-kDa location in subcellular compartments of X$^-$-CGD mutants
(A) NOX2 and p65-kDa were localized using confocal microscopy analysis in control and mutated PLB-985 cells as described in Material and Methods. NOX2 and/or p65-kDa were visualized in green and calnexin as an endoplasmic reticulum marker (ER) in red. Cellular nuclei were stained with Hoechst 33258 (blue). (B) Colocalization analysis of NOX2/p65-kDa with calnexin was performed using the Leica confocal software. Cells presenting a colocalization of NOX2/p65-kDa with calnexin are in yellow (upper right quarter). The same observations were obtained in at least two independent experiments.

Figure 5 Co-immunoprecipitation of the precursor p65-KDa and p22^{phox} from X$^-$-CGD PLB-985 cells
After co-immunoprecipitation of the precursor p65-kDa and p22^{phox} as described in the Material and Methods section, the same amount of proteins of the initial soluble extract fractions (SE), the flow-through of the column with the CS9 antibody (−) and the positive fraction collected after washing with

the sample buffer for SDS PAGE (**+**) were assessed by immunoblot analysis using monoclonal antibodies 48 and 449. HC IgG1 and HL IgG1 indicate positions of the heavy and light chains, respectively, of immunoglobulin. Black boxes indicate the presence or absence of the precursor p65-KDa and $p22^{phox}$ in the positive fraction (**A**) Control cell lines were the WT NOX2 PLB-985 cells in which p65-KDa and $p22^{phox}$ are associated in the positive fraction, the H101Y mutant PLB-985 cells where the mutation affects the p65-kDa and $p22^{phox}$ association. (**B**) Group A X^{-}-CGD mutants with an abnormal accumulation of the precursor p65-kDa. (**C**) Group B X^{-}-CGD mutants with mutations in the FAD binding site. The same observations were obtained in at least three independent experiments.

Figure 6 Ribbon representation of the 3D model of the NOX2 dehydrogenase domain
(A) X^{-}-CGD mutated residues H338 and P339 are located in the binding site for the FAD isoalloxazine ring. H338Y and P339H mutations contribute to disturbing the catalytic site of NOX2 and the localization of NOX2/$p22^{phox}$ to the plasma membrane. **(B)** X^{-}-CGD mutated residues E309, I325 and E389 (affecting the p65/$p22^{phox}$ binding) are located in the intermediate region between the membrane and the dehydrogenase domain of NOX2. Residues are represented as yellow sticks. NADPH and FAD are also represented as sticks in the CPK colour code. The red circle corresponds to a potential $p22^{phox}$ binding region. The figure was drawn using Pymol software.

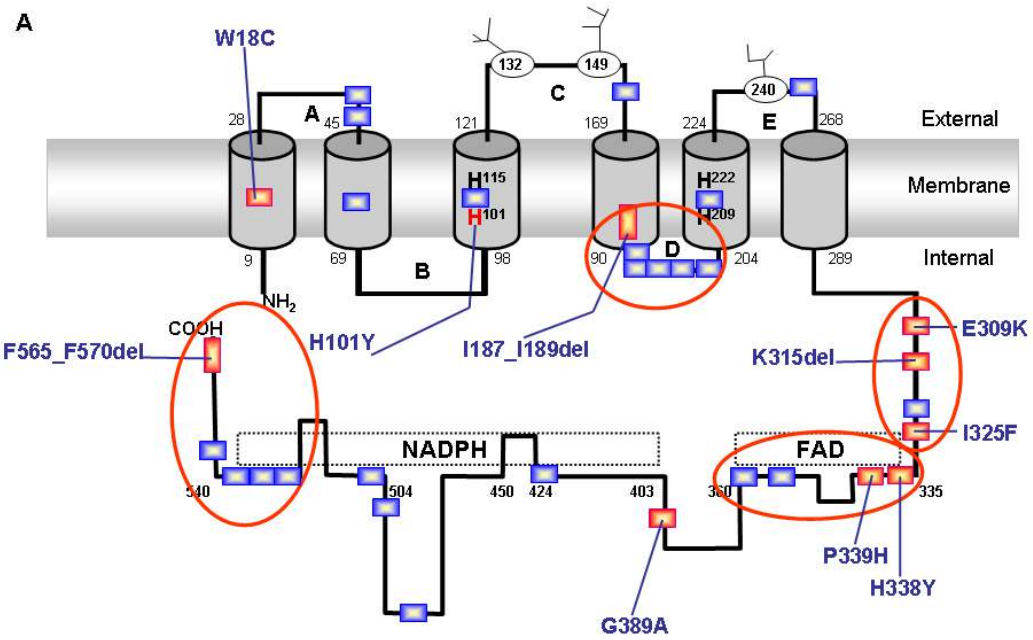
A
W18C
External
Membrane
Internal
A
B
C
D
E
H115
H101
H222
H209
NH2
COOH
F565_F570del
H101Y
I187_I189del
K315del
E309K
I325F
NADPH
FAD
P339H
H338Y
G389A

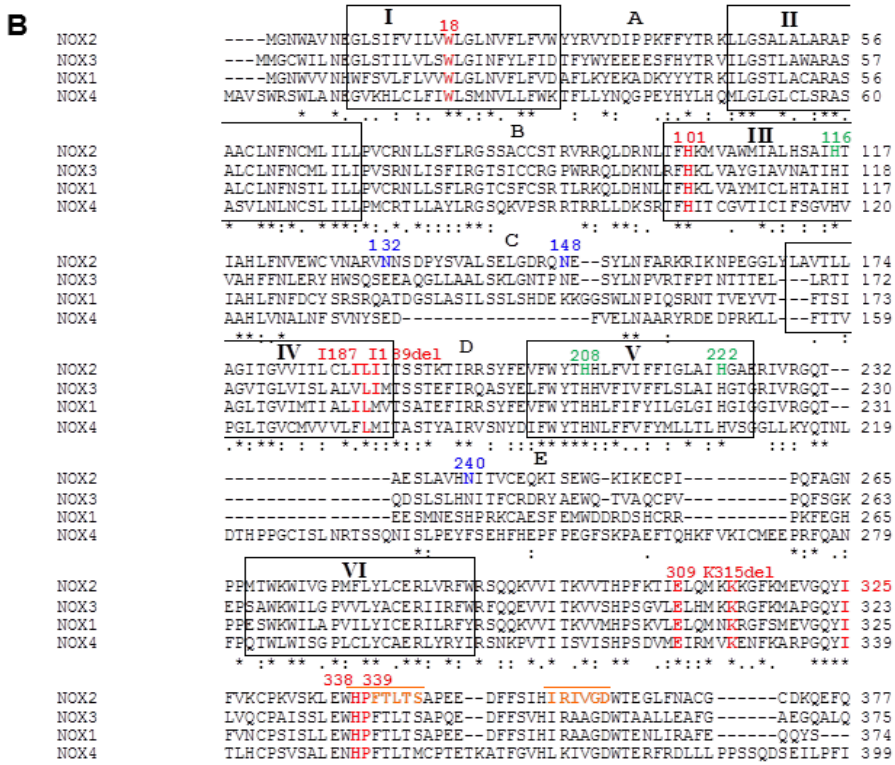
B
I
II
III
IV
V
VI
A
B
C
D
E
I187_I189del
K315del
NOX2
NOX3
NOX1
NOX4

Figure 1

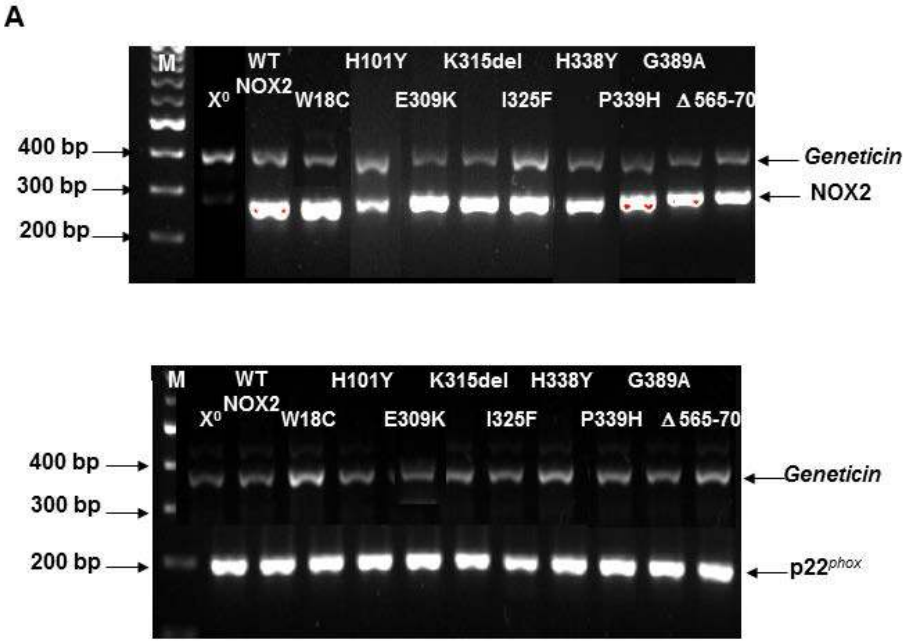
A
M
X⁰
WT NOX2
W18C
H101Y
E309K
K315del
I325F
H338Y
P339H
G389A
Δ565-70
400 bp
300 bp
200 bp
Geneticin
NOX2
M
X⁰
WT NOX2
W18C
H101Y
E309K
K315del
I325F
H338Y
P339H
G389A
Δ565-70
400 bp
300 bp
200 bp
Geneticin
p22phox

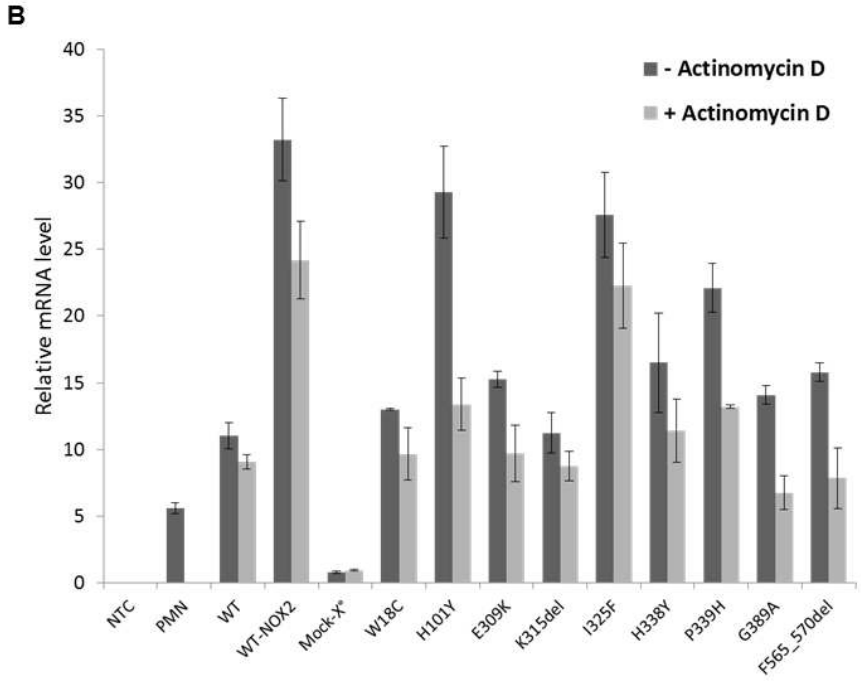
B
- Actinomycin D
+ Actinomycin D
Relative mRNA level
40
35
30
25
20
15
10
5
0
NTC
PMN
WT
WT-NOX2
Mock-X⁰
W18C
H101Y
E309K
K315del
I325F
H338Y
P339H
G389A
F565_570del

Figure 2

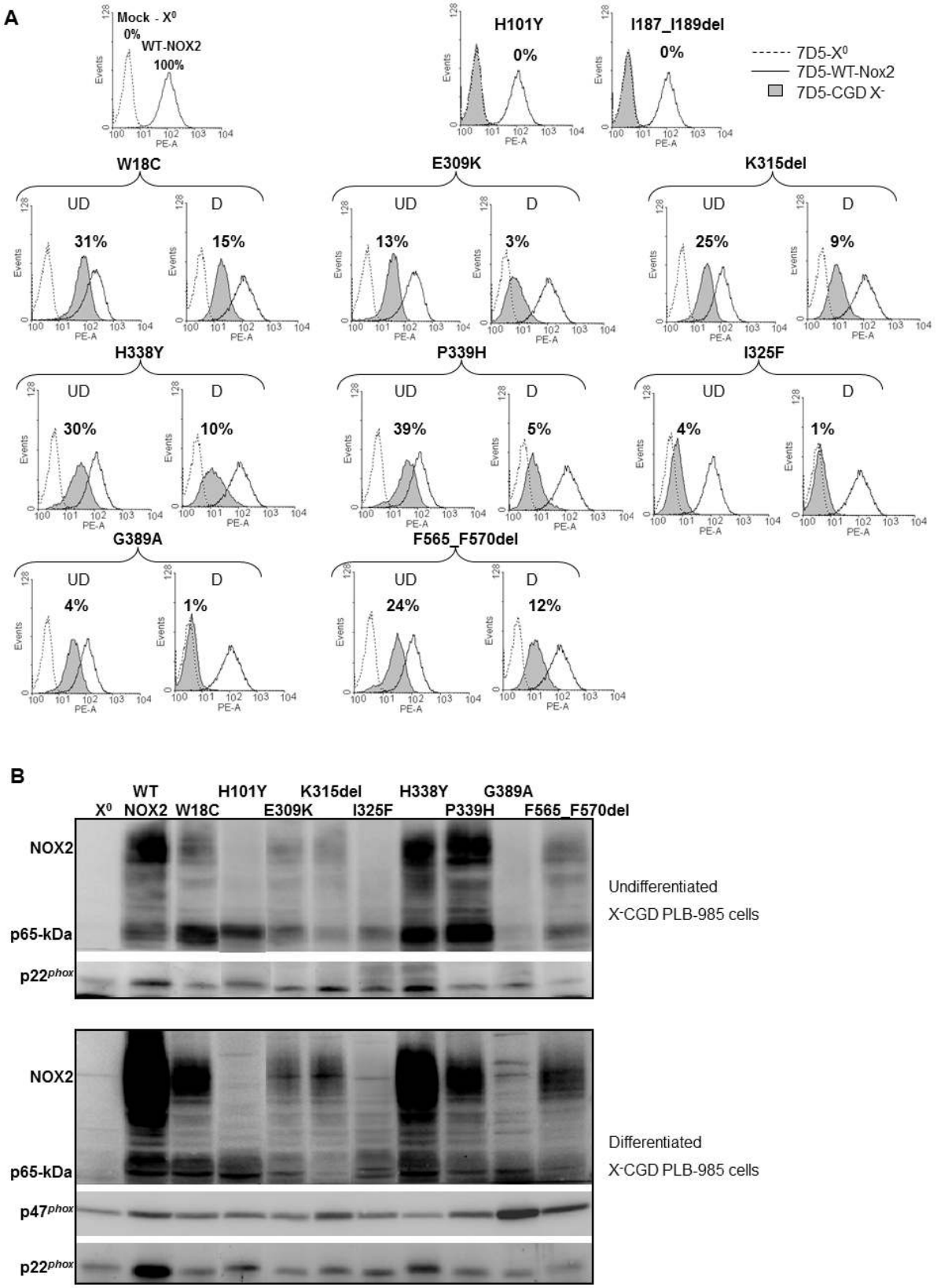
A
Mock - X0
0%
WT-NOX2
100%
H101Y
0%
I187_I189del
0%
7D5-X0
7D5-WT-Nox2
7D5-CGD X-
W18C
UD
31%
D
15%
E309K
UD
13%
D
3%
K315del
UD
25%
D
9%
H338Y
UD
30%
D
10%
P339H
UD
39%
D
5%
I325F
UD
4%
D
1%
G389A
UD
4%
D
1%
F565_F570del
UD
24%
D
12%
Events
PE-A
B
X0
WT NOX2
H101Y W18C
K315del E309K
I325F
H338Y P339H
G389A F565_F570del
NOX2
p65-kDa
p22phox
Undifferentiated
X-CGD PLB-985 cells
NOX2
p65-kDa
p47phox
p22phox
Differentiated
X-CGD PLB-985 cells

Figure 3

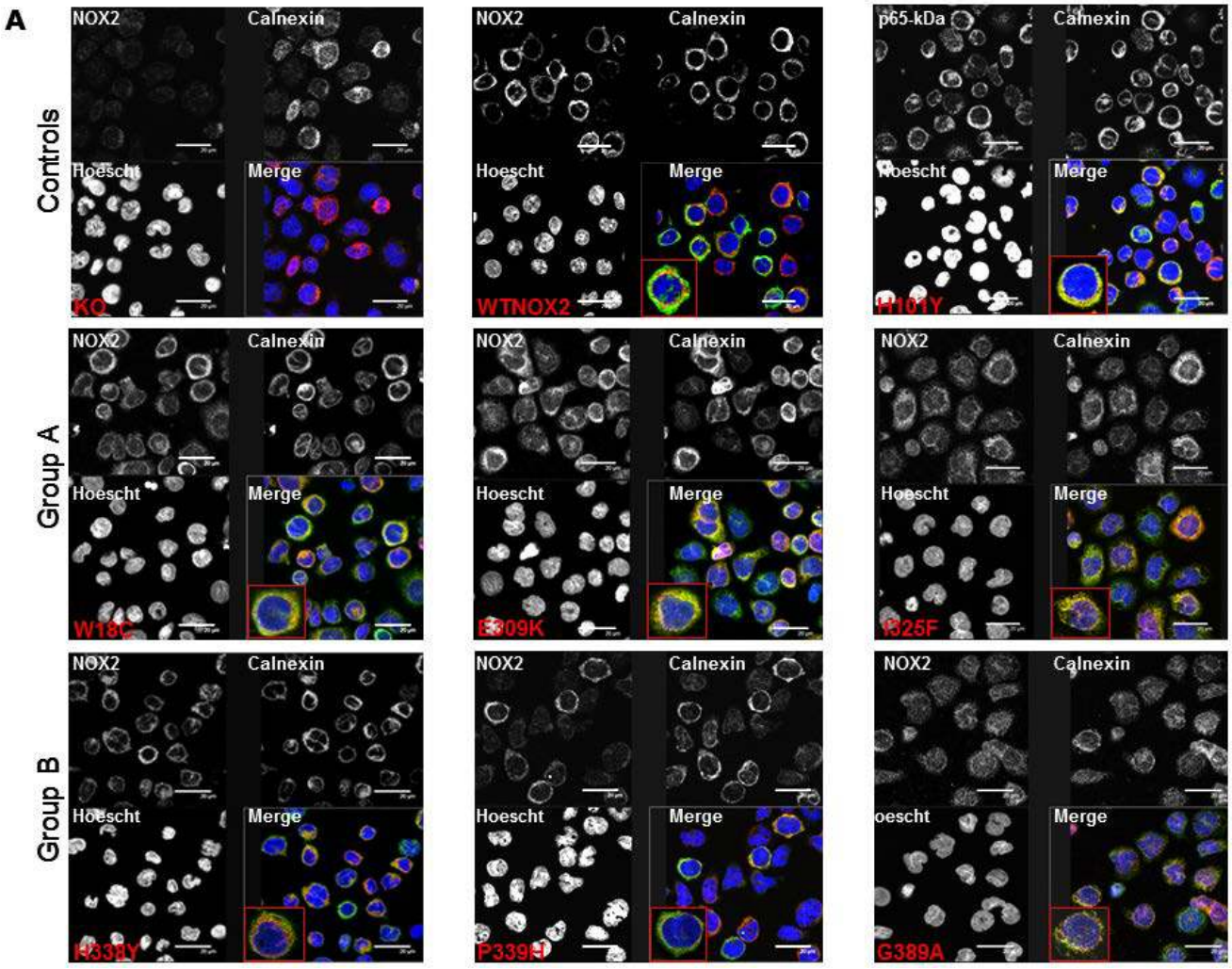
A
Controls
Group A
Group B
NOX2
Calnexin
Hoescht
Merge
KO
WTNOX2
p65-kDa
H101Y
W18C
E309K
I325F
H338Y
P339H
oescht
G389A

Figure 4A

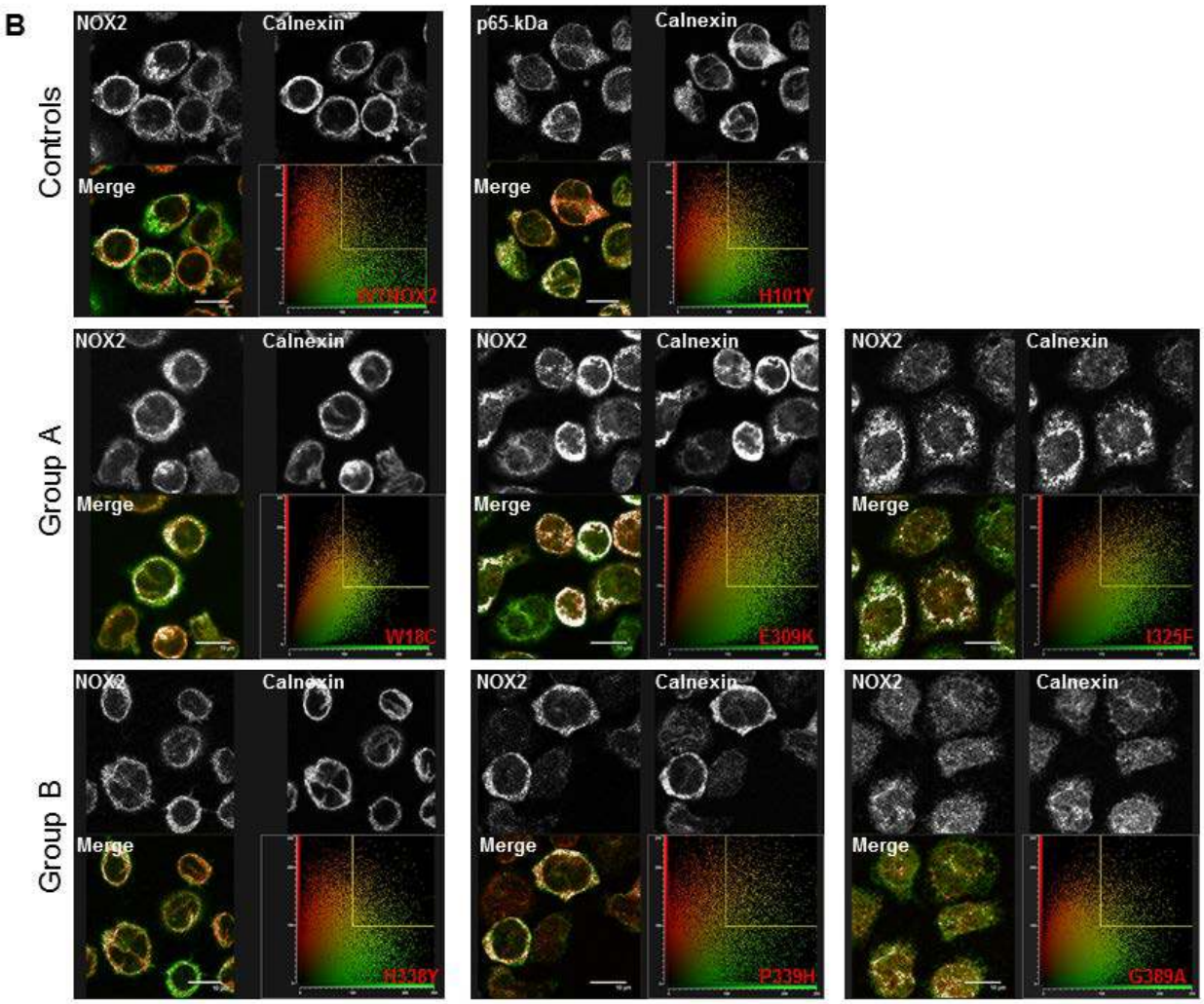
B
Controls
Group A
Group B
NOX2
Calnexin
p65-kDa
Merge
WTNOX2
H101Y
W18C
E309K
I325F
H338Y
P339H
G389A

Figure 4B

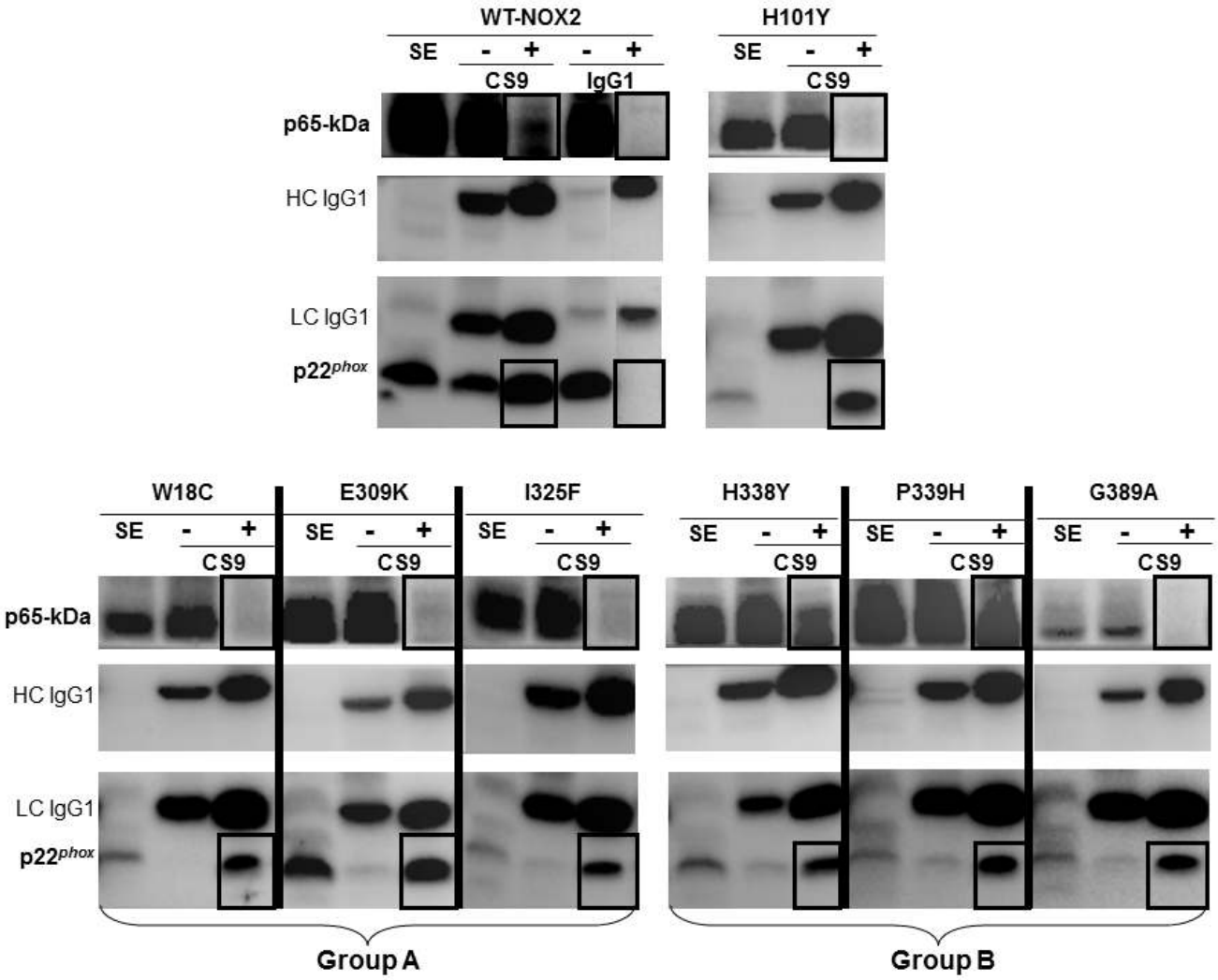
WT-NOX2
H101Y
SE
-
+
CS9
IgG1
p65-kDa
HC IgG1
LC IgG1
p22phox
W18C
E309K
I325F
H338Y
P339H
G389A
Group A
Group B

Figure 5

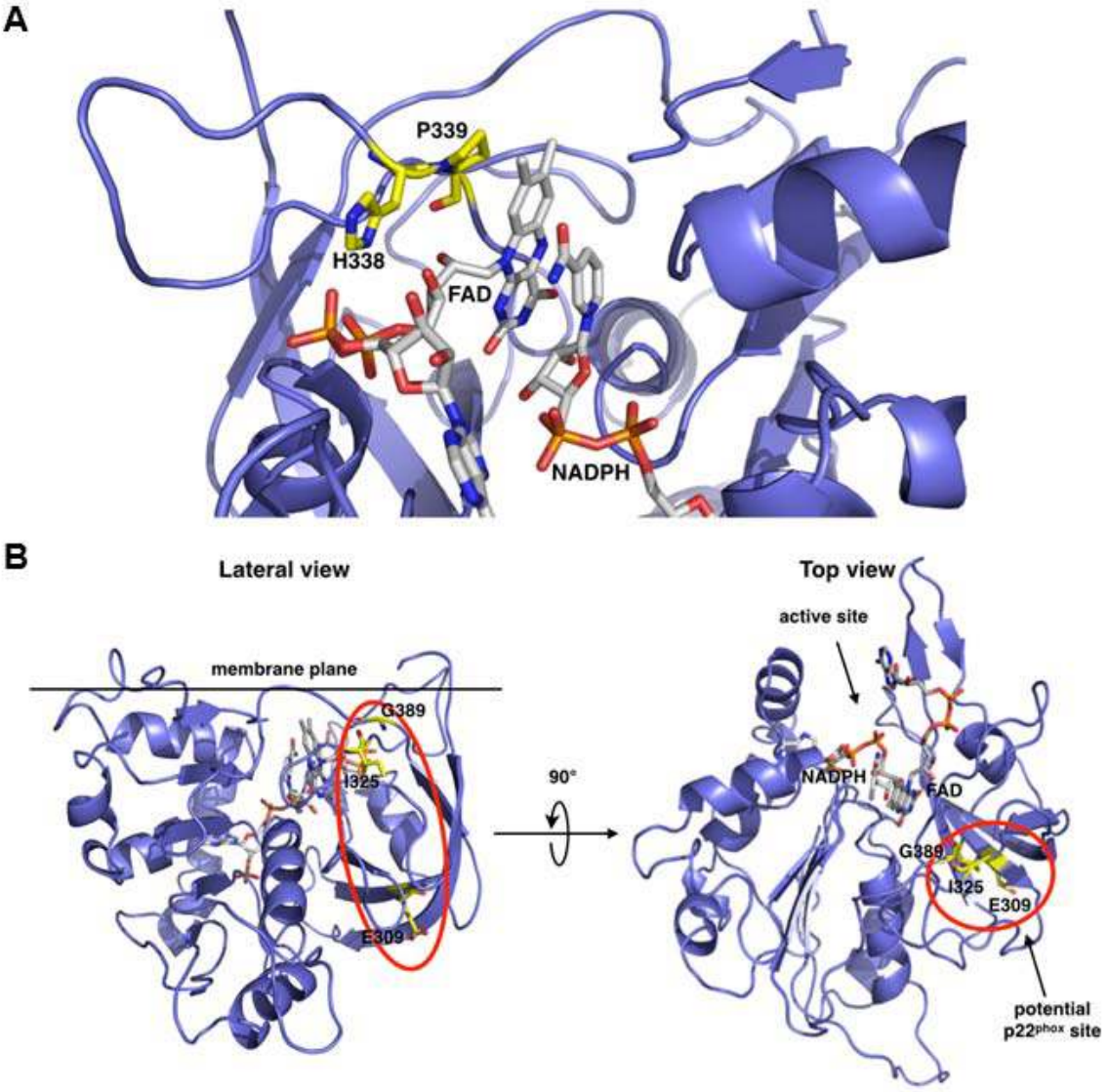
A
P339
H338
FAD
NADPH
B
Lateral view
membrane plane
G389
I325
E309
90°
Top view
active site
NADPH
FAD
G389
I325
E309
potential
p22phox site

Figure 6